

Banner appropriate to article type will appear here in typeset article

Decoupling pressure gradient history effects in turbulent boundary layers through high-Reynolds number experiments

Ahmad Zarei[†], Mitchell Lozier, Rahul Deshpande and Ivan Marusic

Department of Mechanical Engineering, The University of Melbourne, Victoria 3010, Australia

(Received xx; revised xx; accepted xx)

This study provides a carefully controlled examination of the universality of the von Kármán and additive constants associated with the classical logarithmic scaling of the mean streamwise velocity profile in high-friction Reynolds number (Re_τ) turbulent boundary layers (TBLs) subjected to weak-to-moderate adverse pressure gradients (APGs). The analysis leverages a recently developed method for imposing APGs with minimal pressure gradient (PG) history effects in Melbourne's high- Re_τ TBL facility (Deshpande *et al.*, *Phys. Rev. Fluids*, vol. 8, 2023), in combination with direct measurements of local friction velocity via oil-film interferometry. The von Kármán constant is found to remain invariant within experimental uncertainty, while the additive coefficient decreases with both the local APG and PG history, potentially explaining reported variability in logarithmic scalings across the APG TBL literature. The facility enables manual prescription of APGs along the full test section, allowing weak PG history perturbations to be followed by extended recovery regions, while maintaining matched local PG and Re_τ at downstream measurement locations. This experimental configuration allows for systematic decoupling of the effects of Re_τ , local PGs, and PG history, enabling assessment of their individual contributions to single-point turbulence statistics and energy spectra across different TBL regions. Present results at high Re_τ show that PG history influences both small-scale and large-scale motions in the overlap and outer regions, whereas local PGs primarily affect the large-scales. The strongest effects of the local PG occur in the outer region (around 0.4δ , where δ is the boundary layer thickness), while PG history effects extend down to approximately 0.25δ , just above the logarithmic region. In contrast to earlier low- Re_τ studies, neither effect is observed to extend into the near-wall region, suggesting that previous findings may reflect limited scale separation. These measurements yield a high-fidelity dataset and provide a basis for developing composite velocity profile models for APG TBLs that incorporate the distinct influences of Re_τ , local PGs, and PG history.

1. Introduction

Turbulent boundary layers (TBLs) subjected to adverse pressure gradients (APGs) are relevant to a variety of engineering applications, including flows over airfoils and within diffusers. The relevant properties of these APG TBLs are influenced by specific flow conditions, namely the local friction Reynolds number, the local streamwise pressure gradient

[†] Email address for correspondence: a.zarei1994@gmail.com

(PG) and the *history* of streamwise PGs experienced by the TBL upstream of the measurement location (Devenport & Lowe 2022). The local friction Reynolds number, $Re_\tau = \delta U_\tau / \nu$, is a fundamental parameter which also influences (exclusively) the properties of well-behaved, smooth-wall, zero-pressure gradient (ZPG) TBLs (*i.e.*, canonical TBLs; Marusic *et al.* 2015; Sanmiguel Vila *et al.* 2017). Here, δ denotes the boundary layer thickness, U_τ is the mean friction velocity, and ν is the kinematic viscosity. The local streamwise PG is quantified in this study using Clauser's pressure gradient parameter, $\beta = (\delta^* / \rho U_\tau^2)(dP/dx)$, where δ^* is the displacement thickness, ρ is the density, and dP/dx is the local streamwise pressure gradient. Throughout this paper, x and z refer to the streamwise and wall-normal directions, respectively.

An alternate viscous-scaled PG parameter, $p_x^+ = (\nu / \rho u_\tau^3)(dP/dx) = \beta / \delta^{*+}$, has also been considered in previous studies (Nickels 2004). However, for the high- Re_τ TBLs ($Re_\tau \geq 3000$) with weak-to-moderate APGs ($0 \leq \beta < 2$)—the regime considered here— p_x^+ tends towards zero, making β a more appropriate measure of the local PG in this context. The history of streamwise PGs experienced by the TBL upstream of the measurement location will be inferred here from streamwise profiles of the pressure coefficient,

$$C_P(x) = 1 - \frac{U_\infty^2(x)}{U_\infty^2(x=0)}, \quad (1.1)$$

where U_∞ is the freestream velocity and $x = 0$ denotes the wind tunnel test section inlet.

This study focuses on weak-to-moderate APG TBLs, in which $C_P(x)$ profiles reflect streamwise variations in local flow conditions (*e.g.*, $\beta(x) \propto \frac{x}{1-C_P(x)} \frac{dC_P(x)}{dx}$ and $Re_\tau(x) \propto x$). As such, differences in $C_P(x)$ upstream of a given measurement location are interpreted as indicative of qualitative differences in the streamwise PG history experienced by the TBL. While other upstream variations, such as abrupt changes in wall roughness or differing tripping conditions, can also influence APG TBL development and are generally classified as *history* effects (Hanson & Ganapathisubramani 2016), the present study maintains hydrodynamically smooth walls and matched tripping conditions throughout. Accordingly, the discussion of *history* effects in this work is limited exclusively to the streamwise pressure gradient history.

While, the influences of the local flow conditions (*i.e.*, Re_τ and β) on APG TBL properties, specifically turbulence statistics, have been studied over many decades (Clauser 1954), fewer studies have systematically sought to quantify and/or *decouple* the influences of PG history from these parameters. For instance, it is well established that the local streamwise PG, influences the magnitude of both the Reynolds stresses (*e.g.*, the emergence of secondary peaks in the outer region; Skaare & Krogstad 1994; Marusic & Perry 1995; Deshpande & Vinuesa 2024) and the mean streamwise velocity (*e.g.*, increase in the wake factor, Π with β ; Monty *et al.* 2011). However, a number of studies within the past decade (Devenport & Lowe 2022) have demonstrated that the PG history, and the rate of change in upstream PG conditions (Parthasarathy & Saxton-Fox 2023; Gungor *et al.* 2024; Mahajan *et al.* 2025), can influence these mean turbulence statistics on par with the influence of the local PG, motivating the need for further studies to quantify and decouple the influence of local PGs and PG history. As such, PG history effects themselves have recently been investigated in more detail, in both weak-to-moderate (Bobke *et al.* 2017; Vinuesa *et al.* 2017; Pozuelo *et al.* 2022; Romero *et al.* 2023; Gomez & McKeon 2025; Preskett *et al.* 2025) and strong APG conditions (Mahajan *et al.* 2025). However, because these past studies on PG history effects have predominantly been constrained to relatively low Reynolds numbers ($Re_\tau \leq 2000$; Bobke *et al.* 2017; Mahajan *et al.* 2025), open questions remain about how to quantify and

account for the influence of PG history on classical scaling laws, which can only be examined at high Reynolds numbers.

A specific example is the classical logarithmic law, which characterizes the mean velocity profile in the overlap region, and is given by

$$U^+ = \frac{1}{\kappa} \ln(z^+) + B, \quad (1.2)$$

where κ and B are the von Kármán constant and the additive constant, respectively. In this study, these constants are taken as $\kappa = 0.39$ and $B = 4.3$, consistent with values reported for canonical TBLs (Marusic *et al.* 2015). Additionally, throughout this paper, the “+” superscript will be used to denote normalization by viscous velocity (U_τ), length (ν/U_τ), and/or time (ν/U_τ^2). Despite the widespread acceptance of this logarithmic scaling behaviour in the overlap region of high- Re_τ canonical TBLs (Marusic *et al.* 2013; Smits *et al.* 2011), there remains ongoing debate regarding if, and how, κ and B are influenced by local APGs and/or PG history effects (Nickels 2004; Nagib & Chauhan 2008; Knopp *et al.* 2021).

It is important to note that any deviations in mean turbulence statistics from classical scaling laws are only meaningful at sufficiently high Reynolds numbers, where a clear separation exists between the near-wall and outer regions of the TBL, and the overlap region is sufficiently extended to permit unambiguous evaluation of these laws (Smits *et al.* 2011). In the presence of APG, this analysis is further complicated by the fact that, at a minimum, the outer bound of the logarithmic region is influenced by the strength of the pressure gradient (Marusic & Perry 1995). As a result, the combined effects of limited scale separation and/or strong PG history often lead to conflicting reports in the literature regarding potential variations in κ and B for APG TBLs. For example, variations in κ reported by Nickels (2004) and Lee & Sung (2009) may be attributed to low-Reynolds-number conditions. Similarly, changes in the additive constant B have been linked to both the local PG parameter (β) (Nagano *et al.* 1998; Monty *et al.* 2011) and PG history effects (Bobke *et al.* 2017; Gungor *et al.* 2024; Preskett *et al.* 2025). These observations underscore the need for further high-Reynolds-number investigations, which typically require carefully designed, dedicated experimental campaigns.

To that end, numerous high-Reynolds-number experimental studies have been conducted in recent years to investigate the scaling behaviour of APG TBLs, and in particular, the universality of the classical logarithmic law. In these studies, APG conditions have been generated using a variety of methods, including adjustable converging and/or diverging ceilings (Volino 2020; Parthasarathy & Saxton-Fox 2023; Sanmiguel Vila *et al.* 2020), ramp structures (Romero *et al.* 2022; Knopp *et al.* 2021), and wall-normal transpiration (Clauser 1954; Deshpande *et al.* 2023).

A generalized schematic of the streamwise pressure gradient variations commonly encountered in these high- Re_τ APG TBL experiments is shown in figure 1(a). In many cases, the upstream region experiences favourable pressure gradients (FPGs), often introduced by the geometry of ramp structures or ceiling adjustments (Romero *et al.* 2022; Knopp *et al.* 2021). Although these initial PG conditions are setup-dependent, they can influence the downstream development of the TBL. For this reason, any non-zero PG in the farthest upstream region is referred to here as a ‘perturbation’.

This upstream perturbation region is typically followed by a nominally ZPG ‘relaxation’ region, designed to dampen the influence of the upstream PG and re-establish a canonical TBL state. APG conditions are then introduced downstream to form a ‘development’ region where the APG TBL is studied. Most experimental designs include a sufficiently long relaxation region to minimize upstream memory effects and ensure a well-defined baseline prior to the onset of APG conditions. However, despite these efforts, each experimental configuration

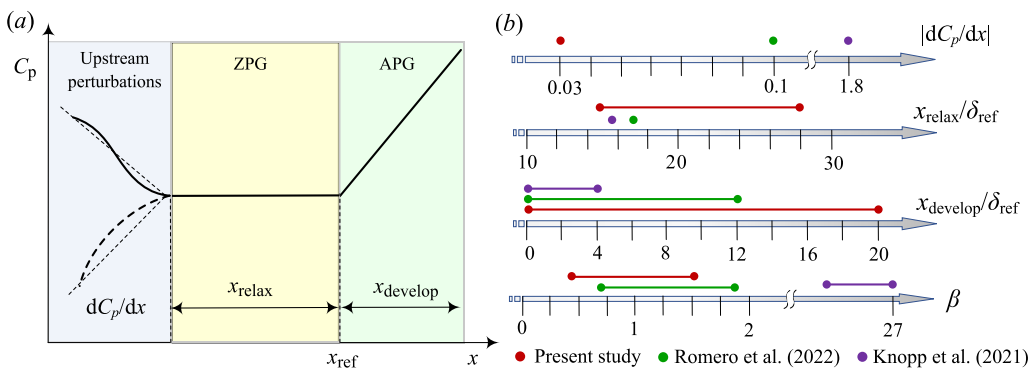


Figure 1: (a) Schematic representation of the different regions of TBL development typically experienced in APG experiments. (b) Comparison of experimental parameters between the present study and those reported by Romero *et al.* (2022) and Knopp *et al.* (2021). $\delta_{ref} = \delta(x = x_{ref})$

imposes a distinct upstream PG history. This variability complicates direct comparisons between different APG TBL datasets, as the development region statistics may retain residual sensitivity to the specific PG history imposed upstream.

As such, any rigorous investigation of the overlap region *e.g.*, quantifying the effect of APGs on classical logarithmic scaling (1.2), requires the satisfaction of three key conditions: (i) the presence of a sufficiently broad overlap region, which necessitates high-Reynolds-number TBLs; (ii) minimal influence of pressure gradient (PG) history effects; and (iii) an independent and accurate estimation of the friction velocity (U_τ). All three of these criteria are met in the present study. In addition, important questions remain regarding the streamwise relaxation lengths required to sufficiently damp PG history effects in high-Reynolds-number APG TBLs—particularly in flows with energized large-scale motions (Marusic *et al.* 2015)—and to recover canonical features such as the classical logarithmic mean velocity profile.

1.1. Present approach

The present study employs a systematic methodology leveraging established large-scale experimental facilities (Marusic *et al.* 2015; Deshpande *et al.* 2023) to generate high- Re_τ weak-to-moderate APG TBLs with user-prescribed upstream PG profiles, consistent with the conceptual framework illustrated in figure 1.

First, this methodology is used to produce TBLs with matched downstream Re_τ and β , but distinct upstream PG histories. This approach enables the decoupling of PG history effects from the influence of local flow conditions on APG TBL development. Importantly, unlike prior experiments, it facilitates a controlled and systematic investigation of PG history effects in high- Re_τ APG TBLs characterized by relatively weak upstream perturbations (low $|dC_p/dx|$), extended relaxation and development regions, and well-matched/controlled local flow conditions downstream (Re_τ and β). As such, any observations made regarding the influence of PG history using this approach should translate to other experiments with stronger PG perturbations and/or shorter relaxation/development regions. Critically, comparisons between APG TBLs with different PG histories here will help to clarify outstanding questions, such as how to appropriately quantify the influence of PG history and what relaxation/development lengths are required to damp upstream PG perturbations, in high- Re_τ experiments.

Finally, the same methodology will be applied to generate high- Re_τ TBLs exhibiting varying weak-to-moderate APGs over an extended downstream fetch, while prescribing

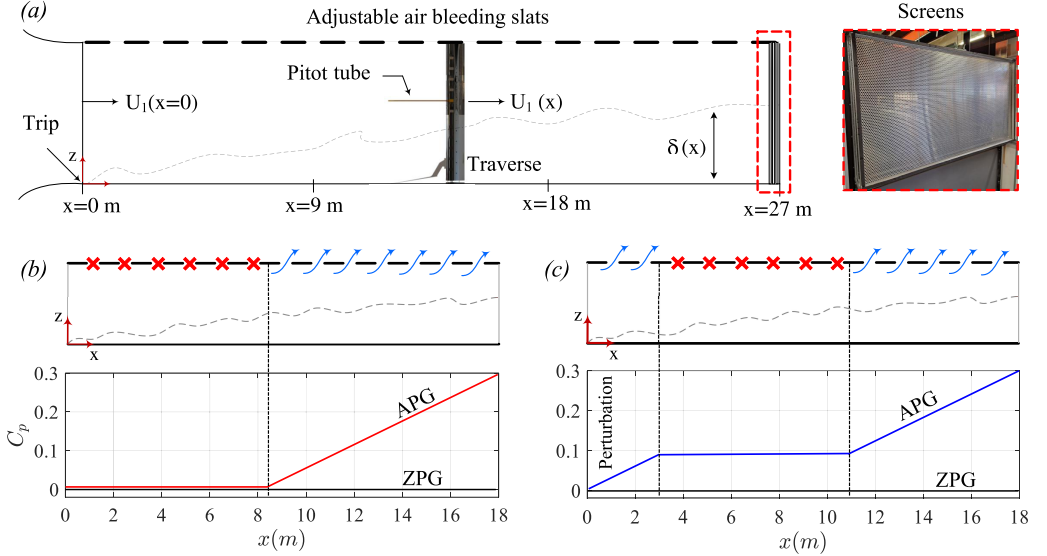


Figure 2: (a) Schematic of the experimental setup established by Deshpande *et al.* (2023), to generate high- Re_τ APG TBLs with controlled pressure gradient histories. Conceptual profile for $C_p(x)$ across the test section to investigate a ZPG/APG TBL with (b) canonical/minimal PG history or (c) with an upstream PG perturbation, following the framework of figure 1(a).

strictly controlled ZPG conditions upstream to minimize PG history effects. This approach addresses limitations in previous studies, where strong upstream PG perturbations and relatively short relaxation/development regions complicated the interpretation of turbulence statistics, including variations in logarithmic law coefficients. The high- Re_τ conditions, weak-to-moderate APGs, minimized PG history achieved here ensure a sufficiently broad overlap region to isolate and investigate the impact of local PGs on the classical logarithmic scaling law. Moreover, the study incorporates an independent friction velocity measurement technique (oil-film interferometry), which is crucial to evaluate normalised turbulence statistics. Together, these features enable a rigorous evaluation of whether the von Kármán constant κ and additive constant B vary in response to weak-to-moderate APGs at high Reynolds numbers.

2. Experimental setup and methodology

The experiments were conducted in the high-Reynolds number boundary layer wind tunnel (HRNBLWT) at the University of Melbourne. The test section has a cross-sectional area of $1.89 \times 0.92 \text{ m}^2$ and a working length of 27 m (figure 2a), enabling the development of physically thick TBLs with high friction Reynolds numbers towards the downstream end. Upstream flow conditioning ensures freestream turbulence intensities remain below 0.4% throughout the test section. The ceiling of the test section is equipped with an array of air-bleed slots spanning the full width, distributed at regular intervals along the streamwise direction. The air-bleed slots allow for controlled removal of air from the test section, driven by the relatively higher static pressure within the test section. This pressure differential is regulated by a series of meshes installed at the test section outlet. A nominal ZPG TBL is established by installing a single high-porosity mesh at the outlet, which produces a small static pressure within the test section, while keeping all air-bleed slots fully open. A detailed characterization of the wind tunnel setup for previous ZPG TBL studies is provided by

Case	x (m)	β	Re_τ	Re_θ	u_τ	δ_{99} (mm)	$\delta_S(\delta)$ (mm)	δ^* (mm)	Symbol
<i>From figure 3(a)</i>									
ZPG	5.1	0	4090	8970	0.50	100.0	124.4	13.2	□
Perturbed	5.1	0	4060	9550	0.47	107.8	132.8	15.1	■
ZPG	8.5	0	5600	12840	0.48	139.0	182.9	19.4	□
Perturbed	8.5	0	5800	13580	0.46	151.6	200.1	21.6	■
ZPG	11.5	0	7000	16880	0.45	174.5	233.3	25.6	□
Perturbed	11.5	0	7400	17840	0.42	193.4	268.5	28.8	■
ZPG	12.8	0	8200	20360	0.48	205.8	273	29.6	□
Perturbed	12.8	0.64	8000	23200	0.41	234.4	296.5	37.8	■
Ref. APG3	12.8	0.65	8000	23400	0.41	230.0	294.8	39.0	■
ZPG	17.4	0	10300	27656	0.43	276.1	370.1	41.0	□
Perturbed	17.4	1.47	10000	34400	0.36	348.8	433.9	65.2	■
Ref. APG3	17.4	1.46	10100	34300	0.35	337.0	440.1	64.3	■
<i>From figure 3(b)</i>									
ZPG	8.5	0	4350	10428	0.33	148.0	203.2	23.3	○
ZPG	8.5	0	6300	14680	0.49	148.8	204.0	21.4	□
APG1	8.5	0	4300	9921	0.35	146.0	193.2	21.4	●
APG1	8.5	0	6500	16112	0.49	152.8	207.3	22.8	■
APG3	8.5	0	4400	9760	0.34	140.5	195.4	20.9	●
APG3	8.5	0	6200	15178	0.47	153.0	199.5	22.4	■
ZPG	12.8	0	5800	14875	0.32	209.9	283.5	33.3	○
ZPG	12.8	0	8300	20360	0.48	205.8	273	29.6	□
APG1	12.8	0.34	5700	15866	0.30	221.9	293.4	37.6	●
APG1	12.8	0.34	8250	21325	0.44	216.3	284.3	32.7	■
APG3	12.8	0.58	5750	17036	0.28	233.4	310.9	41.9	●
APG3	12.8	0.57	8400	22543	0.43	224.7	305.4	36.1	■
ZPG	17.4	0	7300	20048	0.32	276.9	368.1	44.6	○
ZPG	17.4	0	10600	27656	0.43	276.1	370.1	41.0	□
APG1	17.4	0.66	7000	22246	0.27	310.3	399.0	56.0	●
APG1	17.4	0.67	10000	30749	0.39	300.4	387.0	50.9	■
APG3	17.4	1.44	6800	24757	0.25	337.8	420.9	68.1	●
APG3	17.4	1.46	9700	34248	0.36	332.4	419.3	63.7	■

Table 1: Characteristics of the experimental TBLs investigated in the present study.

Marusic *et al.* (2015). Following the methodology of Deshpande *et al.* (2023), the static pressure within the test section can be increased by installing one or more low-porosity (*i.e.*, higher-blockage) screens at the outlet. This configuration produces nominally APG conditions in the upstream portion of the test section when the air-bleed slots remain open,

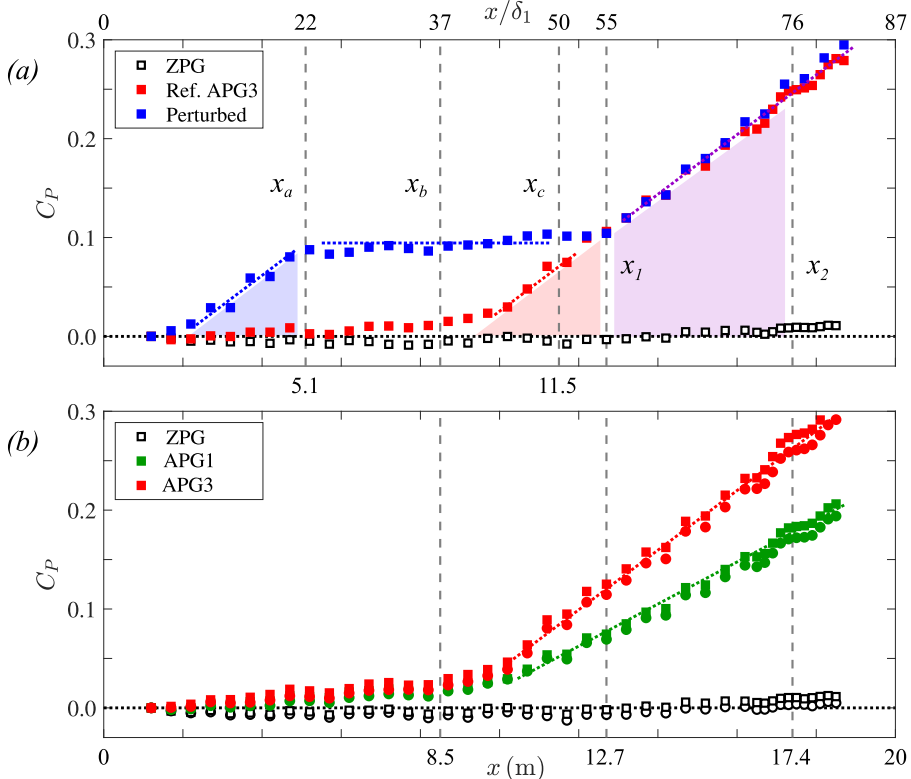


Figure 3: $C_P(x)$ profiles measured for the (a) ZPG, Ref. APG3 and Perturbed APG cases, and the (b) ZPG, APG1 and APG3 cases (see table 1 for exact flow conditions). Vertical dashed lines indicate the locations of streamwise velocity profile and wall shear stress measurements. Here, δ_1 denotes the value of δ at x_1 .

and ZPG conditions when the slots are restricted or closed (see figures 2b,c). This approach, inspired by the seminal work of Clauser (1954), enables the imposition of controlled APG TBLs with minimal physical or geometric modifications to the test section. Figures 2(b,c) schematically illustrate how different PG histories, *i.e.*, streamwise variations in pressure coefficient, can be achieved by selectively opening or closing the air-bleed slots in the upstream region of the test section.

2.1. Approach for imposing distinct upstream pressure gradient histories

Figure 3 presents the experimentally measured pressure coefficient profiles, $C_P(x)$, for various test section configurations, as listed in table 1. For each configuration, the freestream dynamic pressure was measured along the streamwise extent of the test section using a Pitot-static tube mounted at $z = 0.525$ m on the traverse system (figure 2a), enabling quantification of streamwise variations in C_P .

The first configuration corresponds to nominal ZPG conditions throughout the test section, indicated by black symbols in figure 3. Across all ZPG cases tested, variations in $C_P(x)$ remained within 2% along the entire test section. In figure 3 and table 1, square symbols denote inlet unit Reynolds numbers of $U_1(x = 0)/v \approx 9 \times 10^5 \text{ m}^{-1}$, while circle symbols correspond to $\approx 6 \times 10^5 \text{ m}^{-1}$.

To generate APG configurations, either one or three low-porosity screens were added to the outlet, in addition to the baseline high-porosity mesh. These are denoted as APG1 (green

symbols in figure 3b) and APG3 (red symbols in figures 3a,b), respectively. As shown in figure 3(b), both APG1 and APG3 configurations exhibit ZPG conditions upstream of the APG development region ($x < 9$ m), consistent with the setup illustrated in figure 2(b). These cases are referred to as having *minimal upstream history* and serve as reference cases for comparison against those with selectively imposed PG histories. The TBL statistics for APG1 and APG3 were found to collapse with those from the ZPG case at $x = 8.5$ m, confirming the absence of upstream PG influence—consistent with the findings of Deshpande *et al.* (2023).

An additional configuration—the *Perturbed* case—was designed to introduce a controlled upstream PG history. This setup (figure 2c) modifies the open/closed pattern of air-bleed slots in the upstream region, relative to the APG3 case (cf. figures 2b,c). The resulting $C_P(x)$ profile is shown by blue symbols in figure 3(a). For this case, the inlet and downstream flow conditions were matched to the APG3 reference configuration (Ref. APG3), but notable differences in $C_P(x)$ appear upstream ($x < 12$ m) due to the imposed PG perturbation.

The Perturbed case was designed to include a long relaxation region ($5 < x < 12$ m) under nominally ZPG conditions following the initial perturbation. This allows for an investigation into the persistence of downstream flow responses induced by upstream PG history. Moreover, the facility permits sustained APG development over a long streamwise distance, enabling detailed comparison between the Perturbed and Ref. APG3 cases under locally matched flow conditions ($x > 12$ m).

2.2. Streamwise velocity and wall shear stress measurements

Streamwise velocities were measured at selected wall-normal locations using hot-wire anemometry. The hot-wire sensors were manufactured in-house from Wollaston wire, soldered to Dantec 55P15 boundary-layer style probes. The wires were etched to expose a sensing element with diameter $d = 2.5 \mu\text{m}$ and a fixed aspect ratio of $l/d = 200$, corresponding to a nominal sensor length of $l = 0.5$ mm. The resulting viscous-scaled lengths ranged from $l^+ = 11$ to 16 across the cases considered in this study.

To resolve the hierarchy of energetic turbulent scales in the TBL, the sampling time T_S was varied to ensure that a sufficient number of boundary-layer turnover times were captured, satisfying the criterion $T_S U_1 / \delta \geq 20,000$ for all cases. The sampling frequency f_S was fixed at 50 kHz, and the hot-wire signal was low-pass filtered at 25 kHz using an analogue filter to prevent aliasing of high-frequency noise. The resulting viscous-scaled sampling intervals, defined as $t_S^+ = U_\tau^2 / f_S \nu$, ranged from 0.08 to 0.31, which is sufficient to resolve small-scale turbulent motions (Deshpande *et al.* 2023).

The wall-normal hot-wire traverse (figure 2a) had an encoder resolution of $0.1 \mu\text{m}$, enabling precise estimation of relative displacement in the wall-normal direction. However, due to potential wall conduction effects, the first measurement point was limited to $z > 0.2$ mm above the wall. The hot-wire was calibrated before and after each experiment, with intermediate freestream recalibrations performed periodically to correct for hot-wire or ambient drift.

As noted previously, accurate estimation of the friction velocity U_τ is essential in high- Re_τ APG TBL studies, as it serves as a fundamental scaling parameter for turbulence statistics (at least in weak to moderate APG regimes). In the present study, oil-film interferometry (OFI) was used at each measurement location to obtain an accurate and independent estimate of U_τ . Silicone oil droplets ($\mu_{\text{oil}} = 50$ cSt) were placed on optically transparent wall inserts and illuminated from below using a monochromatic light source. The thinning rate of the oil, which is directly related to the mean wall shear stress, was measured by imaging the temporally evolving interference fringes. Further details of the OFI methodology implemented in the present APG TBL experiments are provided in Marusic *et al.* (2024). Taking into account uncertainties associated with oil viscosity calibration, interference

pattern resolution, and potential contamination of the oil droplets, the estimated uncertainty in the measured friction velocity is approximately $\pm 1\%$.

2.3. Experimental dataset summary

Key characteristics for the present experiments, obtained from hot-wire, OFI, and streamwise PG measurements at each location, along with their respective symbols, are presented in table 1 for reference. The recently proposed approach of Lozier *et al.* (2025), based on the streamwise velocity skewness, was employed to determine the representative TBL thickness (δ_S), which is compared against the classical δ_{99} in table 1.

The capability of the proposed methodology for creating controlled PG histories can now be demonstrated quantitatively using the characteristics tabulated in table 1. First, for the cases in figure 3(a), $Re_\tau(x)$ is measured to be nominally matched between the Perturbed and ZPG cases in the upstream section ($x < 12$ m). This is an important condition for investigating the persistence of any deviations observed within the relaxation region that may result from the upstream APG perturbation. In the downstream section ($x > 12$ m) where C_P and dC_P/dx are matched for the Perturbed and Ref. APG3 cases (figure 3a), $Re_\tau(x)$ and $\beta(x)$ are also confirmed to be nominally matched (table 1). This is the critical condition for decoupling the local and upstream PG effects (Bobke *et al.* 2017; Mahajan *et al.* 2025), and quantifying the influence of upstream PG perturbations on the APG TBL development in the downstream development region.

Finally, in figure 3(b), although the local PG (β) varies for the minimal history cases, the Reynolds number is found to be nearly identical between the ZPG, APG1 and APG3 cases with matched upstream inflow conditions, as shown in table 1. This ensures that the effects of the local pressure gradient on TBL statistics and scaling laws can be rigorously evaluated without the influence of varying Reynolds numbers or upstream PG perturbations.

3. Pressure-gradient history effects on high-Reynolds number APG TBLs

3.1. Streamwise mean velocity

We first examine the viscous-scaled mean streamwise velocity profiles (U^+) measured in the relaxation region *i.e.*, at x_a , x_b and x_c (figure 3a), which are shown in figure 4(a). The purely ZPG case is used as a reference. While the local conditions of the Perturbed case are matched with the ZPG case across the relaxation region (table 1), it has experienced an APG perturbation upstream of these measurement locations (figure 3a). This is particularly evident at x_a where the Perturbed mean velocity profile (U^+) in the outer region lies measurably above the ZPG case, despite the Perturbed case experiencing only a weak APG perturbation upstream of x_a (figure 3a). Additionally, the Perturbed mean velocity profile in the overlap region falls slightly below that of the ZPG case at x_a . This is made clearer by subtracting the classical logarithmic scaling law (1.2) from these measured mean velocity profiles ($U^+ - U_{log}^+$), which reveals deviations from canonical scaling behaviour for the Perturbed profile in figure 4(b). Although the deviations in the overlap region at x_a are relatively small, and may, at some wall-normal locations, be on the order of a conservative estimate of experimental uncertainty wall-normal locations, there is a consistent trend (which will be further demonstrated in figure 5 and Appendix A). In the outer region, where the maximum deviation from the logarithmic law is observed (analogous to the wake parameter Π), the difference between the reference ZPG and Perturbed cases exceeds the experimental uncertainty, confirming the influence of the upstream APG perturbation at x_a .

It is also noted that the mean velocity profile in the near-wall region remains largely unaffected by the upstream APG perturbation, consistent with the findings of Bobke *et al.*

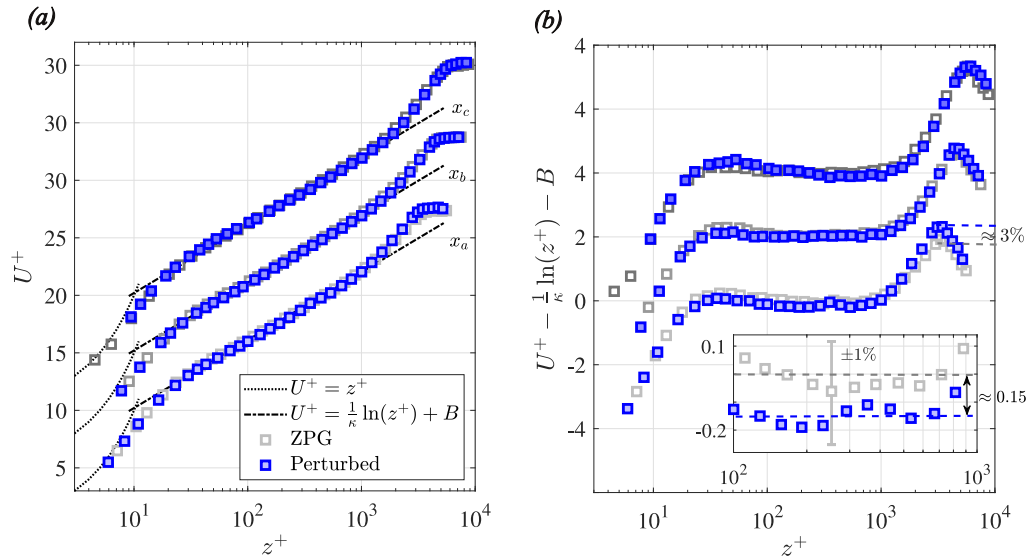


Figure 4: (a) Profiles of mean streamwise velocity, and (b) deviations from the classical logarithmic law for the ZPG and Perturbed cases in the relaxation region. Both cases have locally matched flow conditions, but unique PG histories. Note that the profiles for x_b and x_c are plotted after introducing a vertical offset.

(2017) and Pozuelo *et al.* (2022). This set of results collectively demonstrates that the effects of the upstream APG perturbation on the mean velocity persist at x_a , even though the local pressure gradient has returned to nominally ZPG conditions (*i.e.*, $\beta = 0$).

Further downstream, however, after experiencing sustained ZPG conditions within the relaxation region (figure 1), the Perturbed mean velocity profiles collapse with the reference ZPG profiles (see both x_b and x_c in figure 4a). This collapse is further confirmed by figure 4(b), where both the Perturbed and ZPG cases show good agreement with the classical logarithmic law in the overlap region. Although the mean velocity profiles and scaling behaviour of the Perturbed case have recovered to a ‘canonical’ state at x_b and x_c , differences in characteristics such as the TBL thickness (δ , see table 1), and its growth rate ($d\delta/dx$), still persist and are attributed to the initial upstream APG perturbation. For example, across the full relaxation region (*i.e.*, between x_a and x_c where $x_c - x_a = x_{\text{relax}} \approx 28\delta_1$) the growth rate of the Perturbed TBL is 25% greater than the reference ZPG TBL. This observation is significant, particularly considering that the relaxation length here is considerably longer than those reported in comparable high- Re_τ experiments, which have utilised ramp structures to generate APG TBLs (Romero *et al.* 2022; Knopp *et al.* 2021, see figure 1).

We also consider the implications of these observations for quantifying and accounting for differences in PG history in high- Re_τ TBLs. Previous criteria for quantifying PG history (such as the accumulated PG metric (β) introduced by Vinuesa *et al.* 2017) typically consider the integrated flow conditions experienced upstream of the measurement location. Accordingly, the blue shaded region in figure 3(a) represents a qualitative difference in ‘accumulated’ β between the Perturbed and ZPG cases, which would persist throughout the relaxation region if integrated from $x = 0$. While the qualitative difference in accumulated β appears appropriate/relevant at x_a , it also suggests similar differences should be present at x_b and x_c , which is not supported by the above observations. This indicates these metrics may not be sufficient alone, or need to be modified/constrained, in order to effectively quantify PG history effects in high- Re_τ TBLs.

Further downstream, the mean velocity profiles measured in the development region *i.e.*,

at x_1 and x_2 (figure 3a), are shown in figures 5(a,b). In this region, both the Perturbed and Ref. APG3 cases have nominally matched values of Re_τ and β (see table 1); the ZPG case, included for reference, also has a matched Re_τ . The Ref. APG3 and Perturbed cases, however, have distinct PG histories, as highlighted by the shaded red area upstream of x_1 in figure 3(a). Since the mean velocity profiles for all cases collapse at x_b (figure 4a), any PG conditions or perturbations upstream of x_b are not considered in the following analysis of the development region. Consequently, any differences observed between the Perturbed and Ref. APG3 profiles at x_1 and/or x_2 can be attributed solely to the differences in PG history between x_b and x_1 . Specifically, while the local APG conditions are matched, the Perturbed case has experienced primarily ZPG conditions upstream of x_1 , whereas the Ref. APG3 case has undergone steadily increasing APG conditions over a streamwise distance exceeding 10δ upstream of x_1 .

First, the mean velocity profiles very near the wall ($z^+ \leq 20$) appear largely unaffected by either the local or upstream PGs at both x_1 and x_2 , consistent with the findings of Pozuelo *et al.* (2022). The effect of the local APG (β) alone can be observed at x_2 , where significant deviations from the ZPG profile are observed in both the overlap and outer regions for the Ref. APG3 and Perturbed cases, in agreement with Monty *et al.* (2011); Deshpande *et al.* (2023). However, at x_1 , the influence of PG history is also apparent: although both the Perturbed and Ref. APG3 profiles deviate from the ZPG case, they do not collapse with one another, consistent with the observations of Bobke *et al.* (2017). These differences—well-controlled and monotonic—are reflected in the Perturbed mean velocity profile falling between the ZPG and Ref. APG3 profiles across all wall-normal locations in figure 5(a).

We again consider the implications of these observations for quantifying and accounting for PG history in high- Re_τ experiments. Integrated metrics such as $\bar{\beta}$ would suggest that differences between the Perturbed and Ref. APG3 cases should also persist at x_2 ; however, the strong collapse observed across figures 5(b,d,f) does not support this.

While further work is required to develop robust metrics for capturing PG history effects in high- Re_τ TBLs, the development of high- Re_τ APG TBLs with *minimal* PG history (*i.e.*, Ref. APG3) will be investigated in greater detail in section 4.

The influence of local and upstream PGs on classical logarithmic scaling behaviour is further investigated by examining the indicator function ($z^+ dU^+ / dz^+$) of each mean velocity profile, as shown in figures 5(c,d). At both measurement locations, and for all PG cases, a clear plateau is observed in the overlap region ($10^2 \leq z^+ \leq 10^3$), confirming that there is sufficient separation between the near-wall and outer regions to examine classical scaling laws. Additionally, within experimental uncertainty, no systematic changes are observed in the von Kármán coefficient (κ) due to either local or upstream PGs. The differences in mean velocity profiles discussed above—particularly in the outer region—are also reflected in the indicator functions, confirming that the wake parameter (Π) systematically increases with β (figure 5d, Monty *et al.* 2011), and can also be influenced by PG history (figure 5c, Bobke *et al.* 2017). Finally, the classical logarithmic law (1.2) was subtracted from the measured mean velocity profiles, as shown in figures 5(e,f) (in a manner analogous to figure 4b). In the overlap region, a systematic and significant decrease in the magnitude of the additive constant B is observed with increasing β , especially at x_2 . However, PG history is also seen to affect the value of B at x_1 , where the Ref. APG3 and Perturbed cases do not collapse in the overlap region.

3.2. Streamwise normal stress and premultiplied energy spectra

In this section, we investigate the influence of local and upstream PGs on second-order turbulence statistics and the hierarchy of energetic turbulent motions. To this end, it is useful

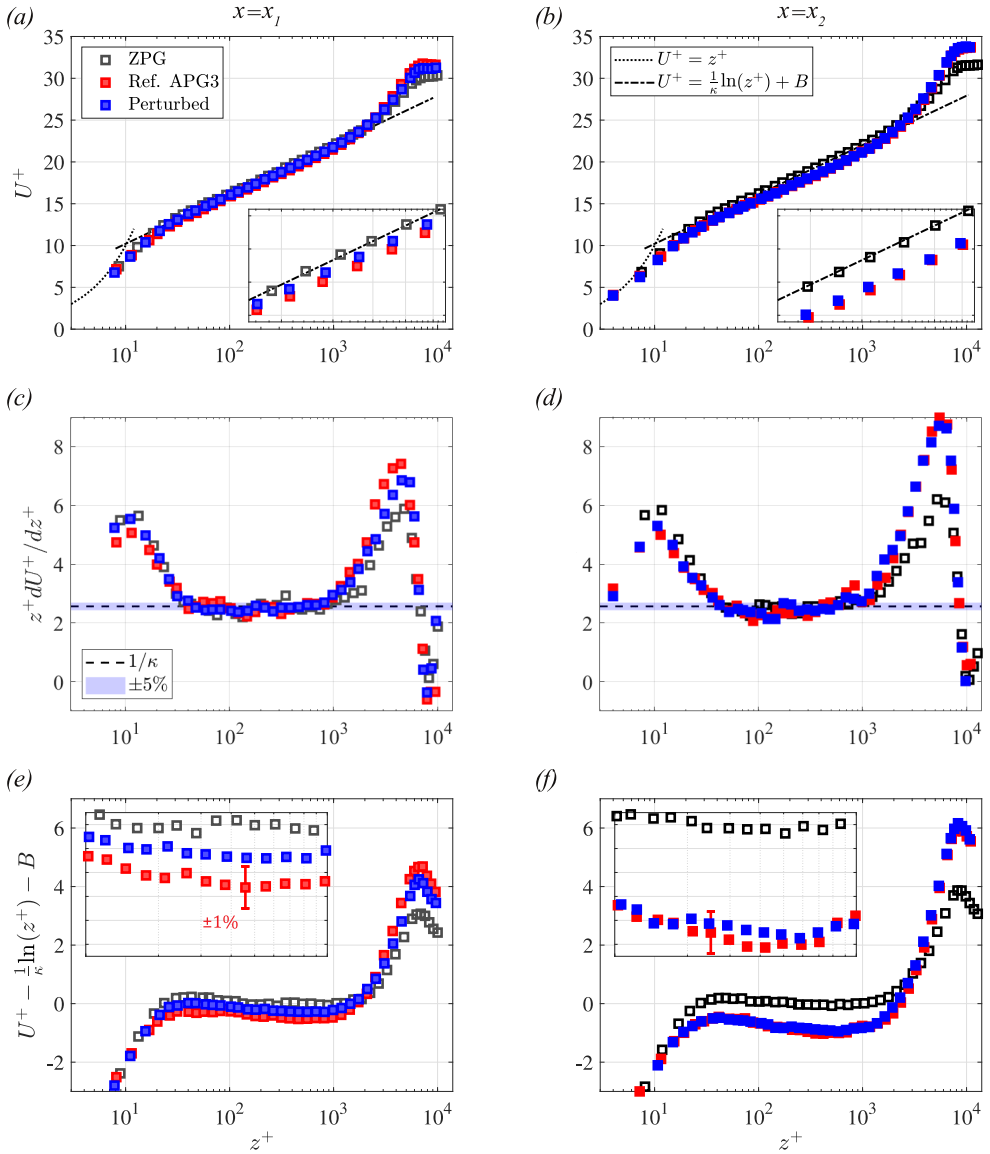


Figure 5: (a,b) Profiles of mean streamwise velocity, (c,d) indicator function, and (e,f) deviations from the classical logarithmic law for the ZPG, Ref. APG3 and Perturbed cases in the development region at (left) $x = x_1$ and (right) $x = x_2$. All cases have locally matched flow conditions, but unique PG histories.

to first contextualise the role of attached-eddy motions and superstructures in high- Re_τ TBLs. These large-scale motions (LSMs) constitute the primary energy-containing motions in the overlap and outer regions, and their contribution becomes increasingly significant with rising Reynolds number (Marusic *et al.* 2013, 2015). In the context of APG flows, it is well established that the magnitude and extent of these LSMs and/or superstructures can be influenced by local PGs (Deshpande *et al.* 2023). Furthermore, recent studies (Bobke *et al.* 2017; Pozuelo *et al.* 2022) have demonstrated that upstream PGs can leave a persistent footprint on other turbulent structures, particularly at lower Reynolds numbers. The objective here is to decouple the effects of local and upstream PGs on the magnitude

and spatial distribution of the hierarchy of turbulent eddies in APG TBLs. The present high- Re_τ experiments offer sufficient scale separation to enable a detailed examination of these influences, especially in relation to LSMs.

The streamwise normal stress profiles ($\overline{u^{+2}}$) measured in the relaxation region are presented in figure 6(a), corresponding to the same cases presented in figure 4(a). To further investigate the distribution of turbulent energy across scales, the premultiplied spectra of streamwise velocity fluctuations ($f\phi_{uu}^+$) have been computed and are plotted as a function of the viscous time scale ($T^+ = U_\tau^2/f\nu$) and wall-normal location (z^+) in figures 6(c,d) which correspond to the streamwise locations x_a and x_b , respectively. Some differences in the streamwise normal stress profiles (figure 6a) and premultiplied spectra (figure 6c) are observed in the outer region ($z^+ \gtrsim 100$) at x_a between the ZPG and Perturbed cases, which can be attributed to differences in their respective PG histories (figures 3a,c). In figures 6(c,d), the horizontal dash-dotted lines denote the Reynolds number dependent characteristic time scale associated with LSMs in canonical TBLs.

At x_a , a secondary spectral peak appears for the Perturbed case (figure 6c), located slightly below this line—*i.e.*, at smaller time scales—highlighting the influence of the upstream APG perturbation (Deshpande *et al.* 2023). This spectral feature corresponds with the elevated outer-region turbulence intensity in the Perturbed normal stress profile and reinforces the conclusion that the upstream PG perturbation leaves a measurable footprint at this location.

Further downstream, however, at x_b , both the normal stress profiles (figure 6a) and premultiplied spectra (figure 6d) for the ZPG and Perturbed cases collapse, indicating recovery from the upstream PG effects. This collapse also persists at x_c , and analysis at that location is omitted here for brevity. These observations are consistent with the trends noted in the mean velocity profiles, where the influence of the upstream PG perturbation in the Perturbed case is limited to the region upstream of x_b .

To further investigate the influence of upstream PG perturbations on the hierarchy of turbulent scales, spectra corresponding to the outer region ($z^+ = 0.4Re_\tau$; vertical dashed lines in figures 6c,d) are plotted in figure 6(b) for x_a and x_b . Here, $0.4Re_\tau$ is approximately equivalent to $0.5\delta_{99}^+$, for reference, and this particular wall-normal location was chosen because it has previously been noted for being strongly influenced by local PGs (Deshpande *et al.* 2023). While the spectra at this wall-normal location collapse at x_b , the influence of the upstream APG perturbation on the Perturbed case can be seen across a broad range of time scales at x_a . However, the “inner-peak” of $\overline{u^{+2}}$ and the associated characteristic wall-normal location/scale in the spectrograms ($z^+ = 15, T^+ = 100$) remain unaffected by the upstream APG perturbation (figures 6a,c), which is consistent with the findings of Bobke *et al.* (2017); Pozuelo *et al.* (2022). These observations suggest that small-scale motions in the near-wall region respond more rapidly to changes in the local PG conditions—*i.e.*, they are less sensitive to PG history—than the LSMs and small-scale turbulence in the outer region. This behaviour is consistent with previous findings (Marusic *et al.* 2015; Sanmiguel Vila *et al.* 2020; Gungor *et al.* 2024; Mahajan *et al.* 2025).

We now investigate the influence of local and upstream PGs farther downstream in the development region, *i.e.*, at x_1 and x_2 . Consistent with observations from the relaxation region, the normal stress profiles in the near-wall region, specifically around the inner-peak where small-scale motions are dominant, collapse well across all cases (figures 7a,b). However, the effects of PGs are clearly evident in the outer region where LSMs are dominant (vertical dashed lines again indicate $z^+ = 0.4Re_\tau$). At x_2 , the Perturbed and Ref. APG3 cases are matched, but both deviate strongly from the ZPG case across a broad wall-normal range in the outer region (figure 7b), highlighting the effect of local PGs (Deshpande *et al.* 2023).

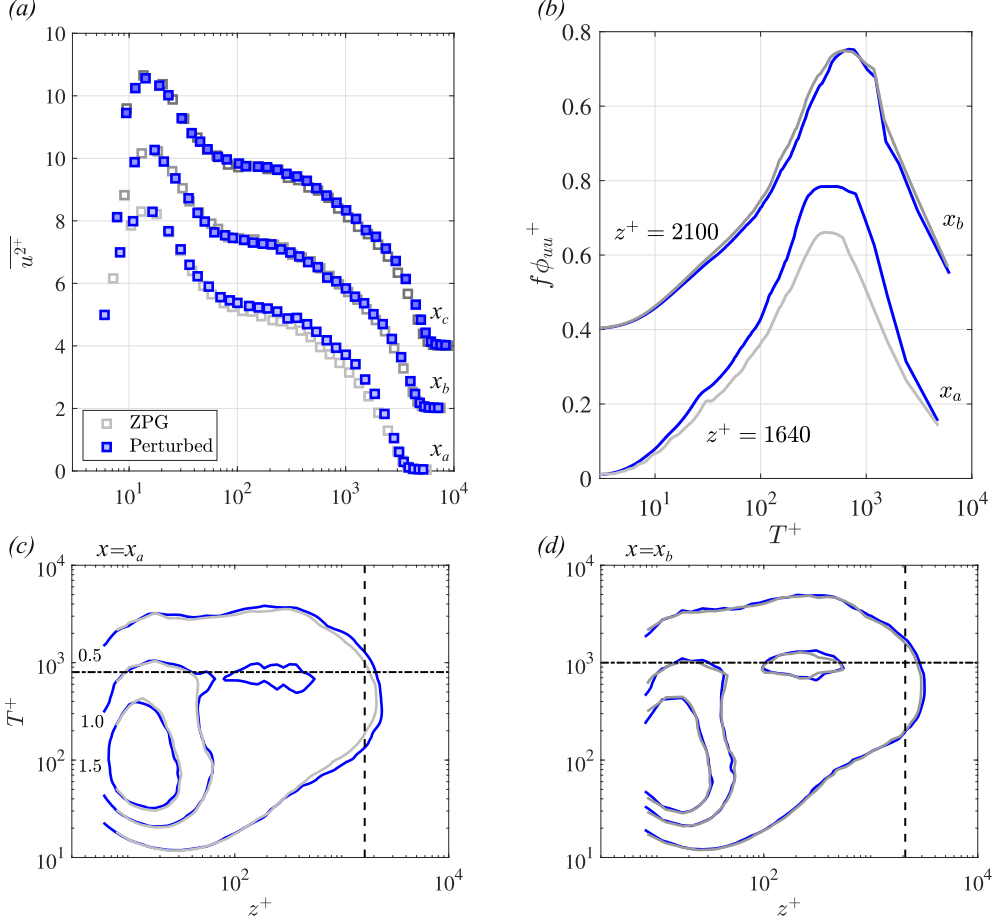


Figure 6: (a) Profiles of streamwise normal stress for the ZPG and Perturbed cases in the relaxation region. Premultiplied energy spectra ($f\phi_{uu}^+$) at (c) $x = x_a$ and (d) $x = x_b$. Vertical dashed lines indicate $z^+ = 0.4Re_\tau$. Horizontal dot-dashed lines denote $T^+ = 4.8\delta^+ / U_\infty^+$. (b) Premultiplied spectra at a single wall-normal location corresponding to the vertical dashed lines in (c,d). Note that the profiles for x_b and x_c are plotted after introducing a vertical offset in (a), while the same is done for the line spectra at x_b in (b).

In contrast, at x_1 , while the Ref. APG3 case clearly departs from the ZPG case in the outer region (figure 7a), the Perturbed case does not collapse with the Ref. APG3 case, reflecting differences in their PG histories. Specifically, while the magnitude of the normal stress in the outer region has increased for the Ref. APG3 case, the Perturbed case remains nearly matched with the ZPG case, consistent with their respective PG histories immediately upstream of x_1 (figure 3).

To further examine the impact of local and upstream PGs on the TBL structure, the corresponding premultiplied energy spectrograms are shown in figures 7(c,d). Both the ZPG and Ref. APG3 cases display typical distributions of energetic turbulent motions; for instance, the outer spectral peak in the ZPG case aligns with the horizontal dash-dotted line ($T^+ / (U_\tau^2 / U_\infty \nu) = 4.8\delta \approx 6\delta_{99}$; Marusic *et al.* 2015), while the outer peak in the Ref. APG3 case (reflecting the effect of the local APG) aligns with the horizontal dotted line ($T^+ / (U_\tau^2 / U_\infty \nu) = 2.4\delta \approx 3\delta_{99}$; Deshpande *et al.* 2023).

Building on the observations from the streamwise normal stress, the Perturbed case at

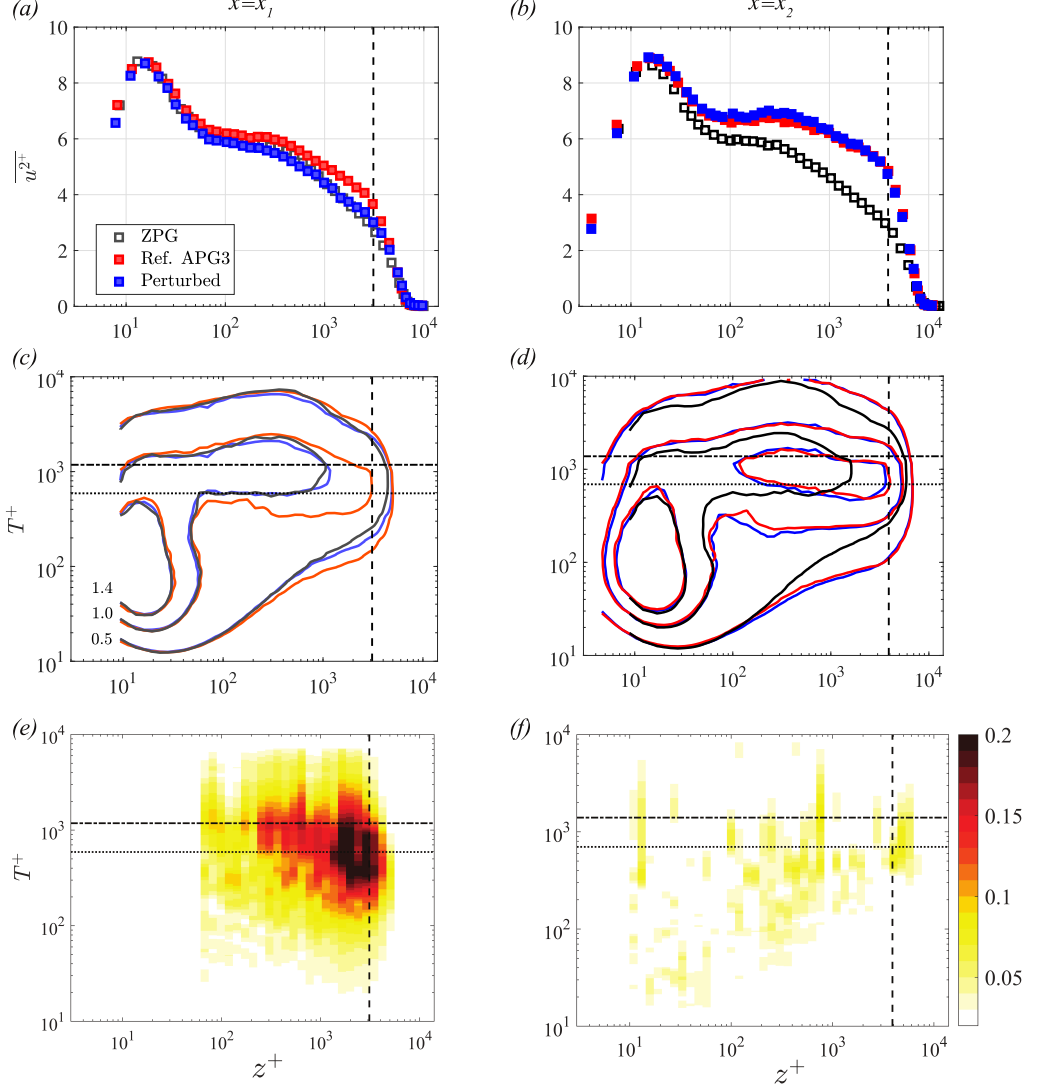


Figure 7: (a,b) Profiles of streamwise normal stress and (c,d) premultiplied energy spectra ($f\phi_{uu}^+$) for the ZPG, Ref. APG3 and Perturbed cases in the development region at (left) $x = x_1$ and (right) $x = x_2$. (e,f) Differences between the Ref. APG3 and Perturbed spectra ($f\phi_{uu, \text{Ref. APG3}}^+ - f\phi_{uu, \text{Perturbed}}^+$). Vertical dashed lines indicate $z^+ = 0.4Re_\tau$. Horizontal dot-dashed lines denote $T^+ = 4.8\delta^+/U_\infty^+$ and horizontal dotted lines denote $T^+ = 2.4\delta^+/U_\infty^+$.

x_1 more closely resembles the ZPG case due to its immediate PG history, whereas at x_2 it matches the Ref. APG3 case. This confirms that upstream PG-related effects no longer persist by x_2 . Additionally, all cases collapse near the wall, consistent with the agreement observed earlier for the inner peak in the normal stress profiles.

To further isolate and examine the influence of PG history, the Ref. APG3 spectra were subtracted from the Perturbed spectra, *i.e.*, $(f\phi_{uu}^+)_{\text{Ref. APG3}} - (f\phi_{uu}^+)_{\text{Perturbed}}$, and the resulting differences are shown in figures 7(e,f). At x_1 , the most prominent differences appear in the outer region, centred around the expected location and scale of APG effects ($z^+ = 0.4Re_\tau$,

$T^+ = 2.4\delta$), demonstrating how the Perturbed case ‘lags’ behind the Ref. APG3 case in APG development due to differences in their immediate PG histories.

Smaller differences are also observed in the logarithmic region at x_1 at larger time scales, supporting the idea that larger-scale motions take longer to respond to PG changes—that is, they retain some ‘memory’ of the upstream PG. At x_2 , however, no significant differences remain in the subtracted spectra, confirming that the two cases are locally matched and that PG history-related effects are no longer evident. These results collectively indicate that while small-scale turbulent motions adjust rapidly to local PG changes, large-scale motions in the logarithmic and outer regions retain a longer memory of immediate PG history in high-Reynolds-number APG TBLs.

Figures 5 and 7 also reveal a unique transitional behaviour in the Perturbed case between x_1 and x_2 , where turbulence statistics and energy distributions initially differ from the Ref. APG3 case but eventually collapse after both cases experience matched PG conditions (figure 3). This motivates an investigation of the streamwise evolution between these locations to isolate the effects of Re_τ , β , and PG history. For each case (Perturbed, ZPG, Ref. APG3), we compute differences in streamwise normal stress and premultiplied spectra between x_1 and x_2 : $\overline{u_{i,x_2}^{+2}} - \overline{u_{i,x_1}^{+2}}$ and $\Delta_i = (f\phi_{uu}^+)_{i,x_2} - (f\phi_{uu}^+)_{i,x_1}$. A shared interpolation grid ensures consistency across datasets. These results are shown in figure 8, where black squares represent the effect of increasing Re_τ (ZPG), red squares show the combined effects of Re_τ and β (Ref. APG3), and blue squares capture the influence of Re_τ , β , and PG history (Perturbed). The differences between these curves isolate each contribution. Stress differences are shown in both viscous units (z^+) and outer scaling (z/δ) to highlight PG effects near the wall and in the outer region, accounting for the change in Re_τ .

As expected (Marusic *et al.* 2015), increasing Re_τ alone raises the normal stress in the overlap and outer regions (figures 8a,b). The addition of an APG energises turbulence at $TU_\infty/\delta \approx 2.4$, with maxima at $z/\delta = 0.4$ (figure 8c), which also corresponds to an increase in stress for the Ref. APG3 case. In contrast, the Perturbed case (figure 8d) shows significantly greater energy growth between x_1 and x_2 , with a broader distribution and peak shifted closer to the wall ($z/\delta \approx 0.25$), indicating a lagged development of APG-related scales due to upstream PG history. While figure 8(c) shows no significant changes in small-scale energy with local PG alone, figure 8(d) reveals a marked increase when PG history is considered. This highlights that PG history influences not only large-scale structures but also significantly impacts small-scale energy, even when the local PG does not.

These results reinforce the need for sufficiently long development regions—especially under rapidly changing PGs—to allow PG history effects to decay. This is essential for accurately studying the streamwise evolution of high- Re_τ APG TBLs and for developing predictive models that reliably capture local effects.

3.3. Reynolds number dependence of PG history effects

One of the key features of the present study is the high- Re_τ condition, which enables clear separation between the near-wall and outer regions of the TBL, as well as between small- and large-scale motions. By decomposing the fluctuating streamwise velocity component (u) into small-scale (u_S) and large-scale (u_L) contributions, we can further examine how PG history affects different turbulent scales and regions.

To highlight the importance of high Re_τ in resolving such effects, we compare the Perturbed and Ref. APG3 cases at x_1 , which have matched local flow conditions ($Re_\tau \approx 8000$, $\beta \approx 0.64$; see figure 9b). For context, we also consider low- Re_τ numerical data from Bobke *et al.* (2017) and Pozuelo *et al.* (2022), with similarly matched local flow parameters ($Re_\tau \approx 500$, $\beta \approx 1$; figure 9a). The influence of Re_τ and β on $\overline{u_S^{+2}}$ and $\overline{u_L^{+2}}$ has been well documented (e.g.

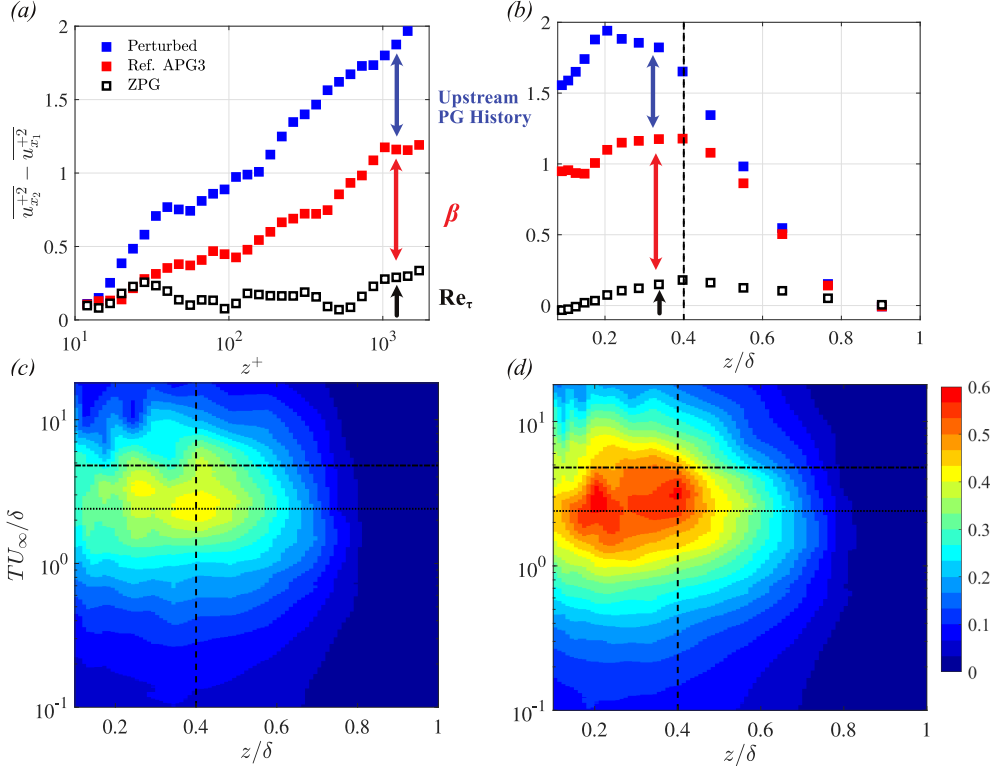


Figure 8: Profiles of the change in streamwise normal stress between x_2 and x_1 for (a) inner scaled and (b) outer scaled wall-normal distances. Differences between the premultiplied energy spectra at x_2 and x_1 ($f\phi_{uu,x_2}^+ - f\phi_{uu,x_1}^+$) for (c) the Ref. APG3 case and (d) the Perturbed case. Vertical dashed lines indicate $z/\delta = 0.4$. Horizontal dot-dashed lines denote $TU_{\infty}/\delta = 4.8$ and horizontal dotted lines denote $TU_{\infty}/\delta = 2.4$.

Lozier *et al.* 2024; Deshpande *et al.* 2023); however, the present methodology allows us to isolate the specific contribution of PG history, independent of these parameters. To perform the decomposition, an appropriate cutoff timescale (T_c^+) must be selected based on the premultiplied energy spectra. Following established practice (Lozier *et al.* 2024; Deshpande *et al.* 2023), we adopt $T_c^+ = 350$, such that u_S includes fluctuations with $T^+ < T_c^+$ and u_L includes those with $T^+ \geq T_c^+$. The analysis was also repeated using a spanwise wavelength-based filter with a cutoff $\lambda_y^+ = 300$ —a common approach in the literature (Deshpande *et al.* 2023; Gungor *et al.* 2024; Mahajan *et al.* 2025)—where $\lambda_y = 2\pi/k_y$ and k_y is the spanwise wavenumber. Both methods yielded consistent results, confirming that the findings are not sensitive to the specific decomposition approach used.

First, both the experimental and numerical datasets show good collapse of the small-scale contributions near the wall, particularly around the inner peak ($z^+ \approx 15$). In the numerical data, PG history effects on the small-scale contribution appear for $z^+ \geq 100$ (or $0.2Re_\tau$) and extend up to the TBL edge (figure 9a). Similar effects are observed in the experimental data for $z^+ \geq 100$ (figure 9b); however, in this high- Re_τ case, the affected range lies primarily in the overlap region and does not extend to the edge of the TBL.

The experimental results also show PG history influencing the large-scale contributions in the overlap and outer regions. These differences are more pronounced than those seen in

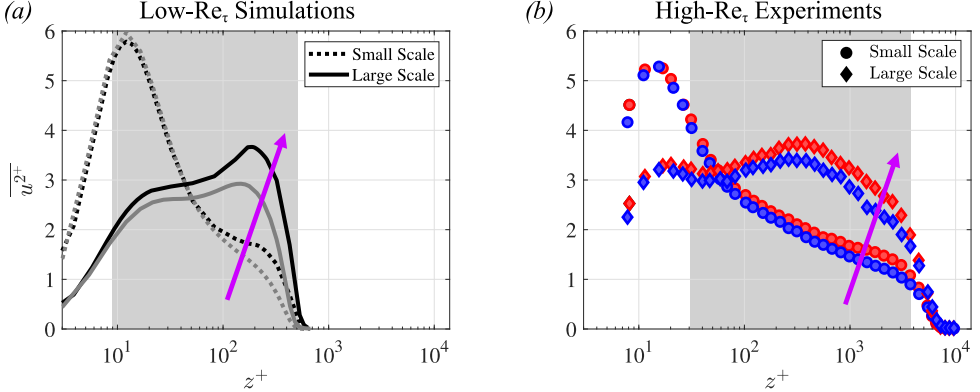


Figure 9: Large- and small-scale contributions to the normal stress for (a) the low- Re_τ numerical datasets of Bobke *et al.* (2017) (black) and Pozuelo *et al.* (2022) (gray) at nominally matched conditions ($Re_\tau \approx 500$ and $\beta \approx 1$) and (b) the high- Re_τ Perturbed (blue) and Ref. APG (red) cases at x_1 with nominally matched conditions ($Re_\tau \approx 8000$, $\beta \approx 0.64$). The shaded region denotes the wall-normal extent where PG history influence is observed.

the small-scale contributions, suggesting that the PG history-related variations in streamwise normal stress (figures 7a,c,e) are primarily due to the energisation of LSMs. In contrast, the numerical results (figure 9a) show large-scale differences not only in the outer region but also closer to the wall ($z^+ \leq 10$), reflecting limited scale separation in the low- Re_τ simulations—a limitation also noted by Harun *et al.* (2013).

Overall, these results indicate that at high Re_τ , PG history primarily affects the overlap and outer regions, leaving the near-wall region largely unaltered. This underscores the need to develop new frameworks that can better capture PG history effects in high- Re_τ TBLs.

4. High-Reynolds number APG TBLs with minimal PG history

We now investigate the development of high- Re_τ mild-APG TBLs with minimal PG history—that is, under strictly ZPG conditions upstream of the measurement region (figure 3b). These experiments enable a rigorous evaluation of local APG effects on classical TBL scaling behaviour, isolated from the influence of strong upstream PG perturbations. To this end, mean streamwise velocity profiles with nominally matched Re_τ but varying β are presented in figure 10(a). Additionally, the indicator function, deviation from (1.2) ($U^+ - U_{log}^+$), and the velocity ratio with respect to the log law (U^+ / U_{log}^+ , following Nagib & Marusic 2025)—are shown in figures 10(b–d), respectively. These measurements correspond to the ZPG, APG1, and APG3 cases at $x = 17.4$, (m) (x_2), with characteristics listed in table 1. Since all three cases share an identical PG history upstream of $x = 8.5$ m (figure 3b), and have nominally matched local Re_τ , any differences in the mean velocity profiles or their scaling are attributable solely to the local APG.

A key observation is the systematic deviation of the APG mean velocity profiles from the ZPG profile in the overlap and outer regions, with the magnitude of deviation increasing with β , as shown in figure 10(a). Similar trends have been reported in both experimental (Nagano *et al.* 1998; Deshpande *et al.* 2023) and numerical studies (Lee & Sung 2009; Yoon *et al.* 2018; Bobke *et al.* 2017; Pozuelo *et al.* 2022; Gungor *et al.* 2024). Figure 10(c) shows that the ZPG mean velocity profile agrees with the classical logarithmic scaling law to within 1% across the entire overlap region, while the APG3 case (highest β) deviates by more than 5%, a statistically significant difference given the experimental uncertainty. These deviations are

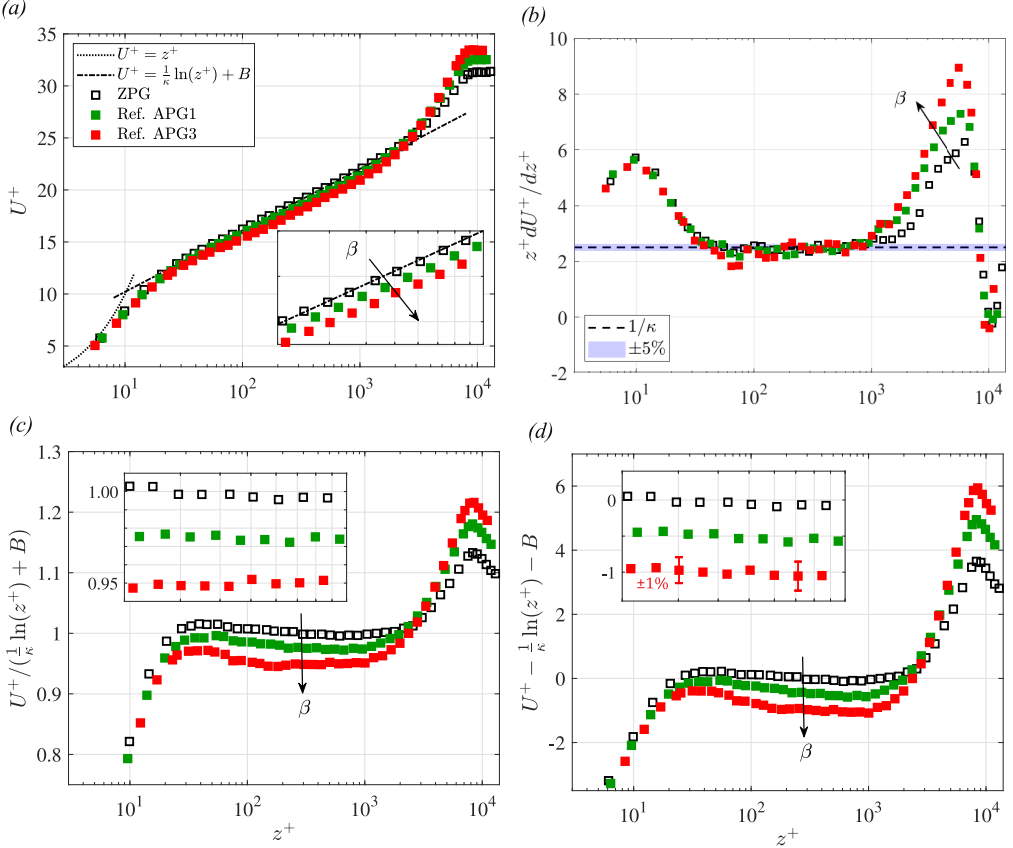


Figure 10: (a) Profiles of mean streamwise velocity for ZPG and APG cases with minimal PG histories at $x = 17.4$ m. All cases have nominally matched $Re_\tau \approx 10000$, but varying β (see table 1). Corresponding (b) indicator functions, (c) ratios with the classical logarithmic law (1,2) and (d) deviations from the classical logarithmic law.

also systematic, as the intermediate APG1 profile falls between the ZPG and APG3 profiles. However, such deviations in the ratio profiles may result from changes in either κ and/or B .

To investigate these coefficients independently, κ is first examined using the indicator function profiles in figure 10(b). A broad wall-normal region with constant indicator magnitude confirms robust logarithmic scaling for all cases, and no systematic or statistically significant change in κ is observed with increasing β (for the high- Re_τ mild-APG cases considered). The additive coefficient B is then isolated using the subtraction profiles in figure 10(d), which show a significant and systematic decrease in the magnitude of B with increasing β . Furthermore, the growing magnitude of these deviations in the outer region reflects a corresponding systematic increase in the wake parameter (Π) with increasing β .

Due to the systematic decrease in B observed for the highest- β cases at $x = 17.4$ m, the additive coefficient was estimated for all present cases (see table 1). Deviations from the classical value of $B = 4.3$ were quantified from the subtraction profiles (figure 10d) by averaging over the wall-normal region where the profiles remain approximately constant (as shown in figure 10b). The resulting values of B as a function of β are presented in figure 11. These results confirm a systematic decrease in B with increasing β , while also indicating that B remains largely independent of Re_τ across the range considered.

According to the high- Re_τ framework proposed by Marusic *et al.* (2013), both κ and B

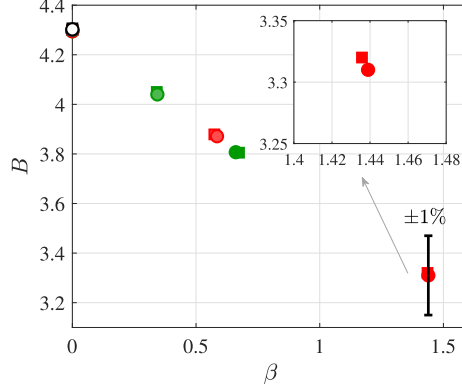


Figure 11: Variation of the classical logarithmic law (1.2) additive coefficient, B , as a function of β for high- Re_τ mild-APG TBLs with minimal PG history effects (see figure 3b and table 1). Note that the circle and square symbols with the same colour correspond to matched β but different Re_τ (see table 1). The inset illustrates that the variations in B arise from the local PG rather than changes in Re_τ .

are considered universal and Reynolds-number invariant for the three canonical flows (ZPG TBLs, pipe, and channel). Notably, this universality has been contested by other studies, such as Nagib & Chauhan (2008); Monkewitz & Nagib (2023). The new experimental results presented here, obtained under systematically varying PG at high Re_τ , clearly indicate that such universality does not necessarily extend to non-canonical flows.

Our results demonstrate that while κ appears to remain universal, the additive constant B is not universal but instead depends on the imposed boundary conditions. Specifically, since the TBL boundary conditions are altered by pressure gradients imposed in the free stream, it is expected that B should vary systematically with both β and PG history. This observation aligns with previous experimental (Nagano *et al.* 1998; Monty *et al.* 2011) and numerical (Bobke *et al.* 2017; Gungor *et al.* 2024) studies reporting reductions in B under APG conditions. However, many earlier investigations were conducted at relatively low Reynolds numbers and/or under significant PG history effects. Moreover, experimental studies have not always determined U_τ via independent measurements, limiting the ability to draw conclusive trends—an issue addressed by the present study. Our experiments suggest that the value of κ remains nominally constant, within experimental uncertainty, for the weak-to-moderate local and historical APG effects considered, consistent with the findings of Knopp *et al.* (2021).

Finally, these results help reconcile why past studies on APG TBLs have sometimes reported conflicting trends. Variations in classical logarithmic law coefficients observed at low Reynolds numbers (e.g., Nickels 2004) or under strong PG history effects can largely be traced to limited scale separation and residual upstream influences—both of which are avoided in the present high- Re_τ study.

5. Conclusions

This study experimentally decoupled and examined the influence of pressure gradient (PG) history on high-Reynolds-number turbulent boundary layers (TBLs) subjected to mild adverse pressure gradients (APGs), using well-resolved hot-wire and OFI measurements. The primary goal was to resolve inconsistencies in existing APG TBL literature by rigorously assessing the universality of the von Kármán constant (κ) and the additive coefficient (B) in the classical logarithmic scaling law for the mean streamwise velocity profile. Leveraging

a recently developed methodology that imposes APGs with minimal PG history effects, we found that κ remains invariant within experimental uncertainty, while the additive coefficient B , systematically decreases with both local PG strength and PG history. These findings explain the variability in logarithmic scaling reported in previous studies, which were likely influenced by low Reynolds numbers, PG history effects, and/or uncertainties in friction velocity measurements.

The experimental facility enabled precise control of APGs with adjustable lengths for both the initial perturbation and the subsequent recovery zone. The study focused on a weak upstream pressure gradient perturbation, followed by an extended relaxation region with a nominally ZPG, leading to a downstream development region characterized by sustained, matched high- Re_τ mild APG conditions. This approach facilitated the systematic separation of PG history effects from local flow parameters (Re_τ and β), enabling detailed analysis of their distinct impacts on turbulence statistics and energy spectra across various TBL regions. Moreover, the relaxation and development zones in this study were longer, and the upstream PG perturbations weaker, than in previous work, allowing these results to be generalized to scenarios with stronger perturbations or shorter relaxation distances. The high- Re_τ conditions also provided sufficient scale separation to investigate how turbulent motions across scales and TBL regions are influenced by PG history.

In the relaxation region, our results confirmed that upstream PG perturbations continue to influence the flow even after the local PG (β) returns to zero, corroborating earlier low- Re_τ findings (Bobke *et al.* 2017; Gungor *et al.* 2024). However, after sufficiently long relaxation distances (26δ), mean velocity and normal stress profiles recovered classical ZPG boundary layer behaviour, while other characteristics such as boundary layer thickness and growth rate remained altered. In the downstream development region, we observed that, even under nominally identical local conditions (matched Re_τ and β), differences in immediate PG history upstream of the measurement location significantly affected the mean velocity profile, particularly within the logarithmic region where classical scaling laws apply. Our data further revealed that PG history influences both small- and large-scale turbulent motions in the overlap and outer regions, while local PGs predominantly impact only large-scale motions. The strongest effects of local PGs were confined to the outer region ($\approx 0.4\delta$), whereas PG history effects extended closer to the wall, reaching just above the logarithmic region ($\approx 0.25\delta$). Unlike prior low- Re_τ studies, neither effect penetrated into the near-wall region, suggesting earlier observations were likely artifacts of insufficient scale separation.

Similar to the relaxation region, after extended development distances (26δ), the flow statistics were found to recover the expected behaviour of APG TBLs. These findings highlight the need to revisit existing criteria in the literature for quantifying PG history effects—such as the accumulated PG history parameter (Vinuesa *et al.* 2017; Mahajan *et al.* 2025)—in the context of high- Re_τ TBLs. While the present study provides initial evidence, additional high- Re_τ experiments encompassing a broader range of PG histories are required to establish a robust and generalizable metric for history effects, which is beyond the current scope.

These findings highlight the importance of establishing experimental TBLs with minimal PG history when investigating the scaling behaviour of high- Re_τ APG flows. The results presented here provide a high-quality dataset and new physical insight, offering a useful basis for developing improved models of the mean velocity profile that distinguish the roles of Re_τ , local PGs, and PG history. Together with existing datasets in the literature and drawing inspiration from the framework laid by Nickels (2004), the present findings provide the foundation for constructing a robust composite profile of APG TBLs that will be presented in the near future.

Acknowledgments. The authors gratefully acknowledge funding from the Office of Naval Research (ONR)

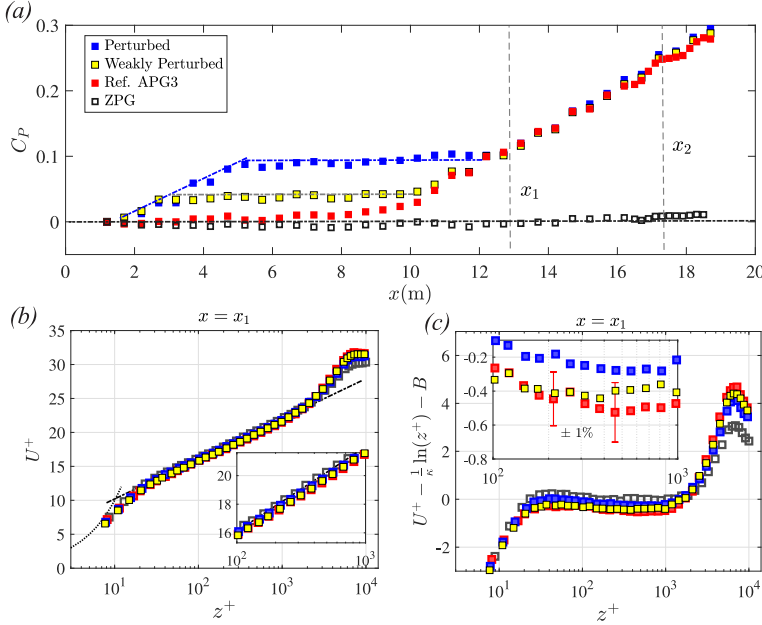


Figure 12: (a) C_P profiles for all cases, including Perturbed and Weakly Perturbed cases with distinct upstream APG histories, (b) mean streamwise velocity profiles and (c) deviations from the classical logarithmic law.

and ONR Global; Grant No. N62909-23-1-2068. R. Deshpande also acknowledges financial support from the Melbourne Postdoctoral Fellowship awarded by the University of Melbourne, and is grateful to A/Prof R. Vinuesa for engaging discussions on APG TBLs.

Declaration of Interests. The authors report no conflict of interest.

Appendix A.

Figure 3 presents a controlled APG perturbation introduced in the upstream region to strategically modify the pressure gradient history of the Perturbed case, in comparison to the reference APG3 case. Additionally, we examine a second case with a relatively weaker upstream APG perturbation (the “Weakly Perturbed” case) to investigate the minimum perturbation strength necessary to observe PG history effects in the turbulence statistics at $x = x_1$. The C_P profiles of these two Perturbed cases are shown in figure 12(a), along with the Ref. APG3 and ZPG cases. At x_1 , Re_τ and β are still nominally matched across all cases, including the Weakly Perturbed case.

The mean velocity profiles and their deviations from the classical logarithmic scaling law are presented in figures 12(b,c). The mean velocity and deviation profiles (in the overlap region) for the Weakly Perturbed case fall between those of the Ref. APG3 and Perturbed cases, showing a systematic trend consistent with the earlier discussion. However, the differences between the Weakly Perturbed and Ref. APG3 cases fall within experimental uncertainty. As such, the Weakly Perturbed case is not considered for further analysis.

REFERENCES

BOBKE, A., VINUESA, R., ÖRLÜ, R. & SCHLATTER, P. 2017 History effects and near equilibrium in adverse-pressure-gradient turbulent boundary layers. *J. Fluid Mech.* **820**, 667–692.

CLAUSER, F. H. 1954 Turbulent boundary layers in adverse pressure gradients. *J. Aeronaut. Sci.* **21** (2), 91–108.

DESHPANDE, R., VAN DEN BOGAARD, A., VINUESA, R., LINDIĆ, L. & MARUSIC, I. 2023 Reynolds-number effects on the outer region of adverse-pressure-gradient turbulent boundary layers. *Phys. Rev. Fluids* **8** (12), 124604.

DESHPANDE, R. & VINUESA, R. 2024 Streamwise energy-transfer mechanisms in zero-and adverse-pressure-gradient turbulent boundary layers. *J. Fluid Mech.* **997**, A16.

DEVENPORT, W. J. & LOWE, K. T. 2022 Equilibrium and non-equilibrium turbulent boundary layers. *Prog. Aerosp. Sci.* **131**, 100807.

GOMEZ, S. R. & McKEON, B. J. 2025 Linear analysis characterizes pressure gradient history effects in turbulent boundary layers. *J. Fluid Mech.* **1002**, A20.

GUNGOR, T. R., GUNGOR, A. G. & MACIEL, Y. 2024 Turbulent boundary layer response to uniform changes of the pressure force contribution. *J. Fluid Mech.* **997**, A75.

HANSON, R. E. & GANAPATHISUBRAMANI, B. 2016 Development of turbulent boundary layers past a step change in wall roughness. *J. Fluid Mech.* **795**, 494–523.

HARUN, Z., MONTY, J. P., MATHIS, R. & MARUSIC, I. 2013 Pressure gradient effects on the large-scale structure of turbulent boundary layers. *J. Fluid Mech.* **715**, 477–498.

KNOPP, T., REUTHER, N., NOVARA, M., SCHANZ, D., SCHÜLEIN, E., SCHRÖDER, A. & KÄHLER, C. J. 2021 Experimental analysis of the log law at adverse pressure gradient. *J. Fluid Mech.* **918**, A17.

LEE, J.-H. & SUNG, H. J. 2009 Structures in turbulent boundary layers subjected to adverse pressure gradients. *J. Fluid Mech.* **639**, 101–131.

LOZIER, M., DESHPANDE, R., ZAREI, A., LINDIĆ, L., ROWIN, W. A. & MARUSIC, I. 2025 Defining the mean turbulent boundary layer thickness based on streamwise velocity skewness. *arXiv:2502.00157*.

LOZIER, M., MARUSIC, I. & DESHPANDE, R. 2024 Revisiting amplitude modulation in non-canonical wall-turbulence through high-Reynolds number experimental data. *Phys. Rev. Fluids* **9** (12), 124602.

MAHAJAN, A., DESHPANDE, R., GUNGOR, T. R., MACIEL, Y. & VINUESA, R. 2025 Upstream history quantification and scale-decomposed energy analysis for weak-to-strong adverse-pressure-gradient turbulent boundary layers. *Int. J. Heat Fluid Flow* **117**, 110004.

MARUSIC, I., ABU ROWIN, W., LOZIER, M., LINDIĆ, L., ZAREI, A. & DESHPANDE, R. 2024 Turbulent/non-turbulent interface in high Reynolds number pressure gradient boundary layers. In *IUTAM Symposium on Turbulent/Non-Turbulent Interface in Turbulent Shear Flows*, pp. 3–17.

MARUSIC, I., CHAUHAN, K. A., KULANDAIYELU, V. & HUTCHINS, N. 2015 Evolution of zero-pressure-gradient boundary layers from different tripping conditions. *J. Fluid Mech.* **783**, 379–411.

MARUSIC, I., MONTY, J. P., HULTMARK, M. & SMITS, A. J. 2013 On the logarithmic region in wall turbulence. *J. Fluid Mech.* **716**, R3.

MARUSIC, I. & PERRY, A. E. 1995 A wall-wake model for the turbulence structure of boundary layers. part 2. further experimental support. *J. Fluid Mech.* **298**, 389–407.

MONKEWITZ, P.A. & NAGIB, H.M. 2023 The hunt for the Kármán ‘constant’ revisited. *Journal of Fluid Mechanics* **967**, A15.

MONTY, J. P., HARUN, Z. & MARUSIC, I. 2011 A parametric study of adverse pressure gradient turbulent boundary layers. *Int. J. Heat Fluid Flow* **32** (3), 575–585.

NAGANO, Y., TSUJI, T. & HOURA, T. 1998 Structure of turbulent boundary layer subjected to adverse pressure gradient. *Int. J. Heat Fluid Flow* **19** (5), 563–572.

NAGIB, H. & MARUSIC, I. 2025 A method for evaluating relations of turbulent normal-stresses by experimental data over a wide range of Reynolds numbers. *J. Fluid Mech.* **1016**, A24.

NAGIB, H. M. & CHAUHAN, K. A. 2008 Variations of von Kármán coefficient in canonical flows. *Phys. Fluids* **20** (10).

NICKELS, T. B. 2004 Inner scaling for wall-bounded flows subject to large pressure gradients. *J. Fluid Mech.* **521**, 217–239.

PARTHASARATHY, A. & SAXTON-FOX, T. 2023 A family of adverse pressure gradient turbulent boundary layers with upstream favourable pressure gradients. *J. Fluid Mech.* **966**, A11.

POZUELO, R., LI, Q., SCHLATTER, P. & VINUESA, R. 2022 An adverse-pressure-gradient turbulent boundary layer with nearly constant. *J. Fluid Mech.* **939**, A34.

PRESKETT, T., VIRGILIO, M., JAISWAL, P. & GANAPATHISUBRAMANI, B. 2025 Effects of pressure gradient histories on skin friction and mean flow of high Reynolds number turbulent boundary layers over smooth and rough walls. *J. Fluid Mech.* **1010**, A30.

ROMERO, S., ZIMMERMAN, S., PHILIP, J. & KLEWICKI, J. 2023 Velocity spectra and scale decomposition of

adverse pressure gradient turbulent boundary layers considering history effects. *Int. J. Heat Fluid Flow* **102**, 109143.

ROMERO, S., ZIMMERMAN, S., PHILIP, J., WHITE, C. & KLEWICKI, J. 2022 Properties of the inertial sublayer in adverse pressure-gradient turbulent boundary layers. *J. Fluid Mech.* **937**, A30.

SANMIGUEL VILA, C., VINUESA, R., DISCETTI, S., IANIRO, A., SCHLATTER, P. & ÖRLÜ, R. 2017 On the identification of well-behaved turbulent boundary layers. *J. Fluid Mech.* **822**, 109–138.

SANMIGUEL VILA, C., VINUESA, R., DISCETTI, S., IANIRO, A., SCHLATTER, P. & ÖRLÜ, R. 2020 Experimental realisation of near-equilibrium adverse-pressure-gradient turbulent boundary layers. *Exp. Therm. Fluid Sci.* **112**, 109975.

SKAARE, P. E. & KROGSTAD, P.-Å. 1994 A turbulent equilibrium boundary layer near separation. *J. Fluid Mech.* **272**, 319–348.

SMITS, A. J., McKEON, B. J. & MARUSIC, I. 2011 High-Reynolds number wall turbulence. *Annu. Rev. Fluid Mech.* **43** (1), 353–375.

VINUESA, R., ÖRLÜ, R., SANMIGUEL VILA, C., IANIRO, A., DISCETTI, S. & SCHLATTER, P. 2017 Revisiting history effects in adverse-pressure-gradient turbulent boundary layers. *Flow Turbul. Combust.* **99**, 565–587.

VOLINO, R. J. 2020 Non-equilibrium development in turbulent boundary layers with changing pressure gradients. *J. Fluid Mech.* **897**, A2.

YOON, M., HWANG, J. & SUNG, H. J. 2018 Contribution of large-scale motions to the skin friction in a moderate adverse pressure gradient turbulent boundary layer. *J. Fluid Mech.* **848**, 288–311.